Radiomics of Preoperative Multi-Sequence Magnetic Resonance Imaging Can Improve the Predictive Performance of Microvascular Invasion in Hepatocellular Carcinoma

Wan Min Liu[a, e], Xing Yu Zhao[a, e], Meng Ting Gu[a], Kai Rong Song[b], Wei Zheng[b], Hui Yu[b], Hui Lin Chen[c], Xiao Wen Xu[a], Xiang Zhou[a], Ai E Liu[d], Ning Yang Jia[b, f], Pei Jun Wang[a, f]

Abstract

Background: The aim of the study is to demonstrate that radiomics of preoperative multi-sequence magnetic resonance imaging (MRI) can indeed improve the predictive performance of microvascular invasion (MVI) in hepatocellular carcinoma (HCC).

Methods: A total of 206 patients with pathologically confirmed HCC who underwent preoperative enhanced MRI were retrospectively recruited. Univariate and multivariate logistic regression analysis identified the independent clinicoradiologic predictors of MVI present and constituted the clinicoradiologic model. Recursive feature elimination (RFE) was applied to select radiomics features (extracted from six sequence images) and constructed the radiomics model. Clinicoradiologic model plus radiomics model formed the clinicoradiomics model. Five-fold cross-validation was used to validate the three models. Discrimination, calibration, and clinical utility were used to evaluate the performance. Net reclassification improvement (NRI) and integrated discrimination improvement (IDI) were used to compare the prediction accuracy between models.

Results: The clinicoradiologic model contained alpha-fetoprotein (AFP)_lg10, radiological capsule enhancement, enhancement pattern and arterial peritumoral enhancement, which were independent risk factors of MVI. There were 18 radiomics features related to MVI constructed the radiomics model. The mean area under the receiver operating curve (AUC) of clinicoradiologic, radiomics and clinicoradiomics model were 0.849, 0.925 and 0.950 in the training cohort and 0.846, 0.907 and 0.933 in the validation cohort, respectively. The three models' calibration curves fitted well, and decision curve analysis (DCA) confirmed the clinical usefulness. Compared with the clinicoradiologic model, the NRI of radiomics and clinicoradiomics model increased significantly by 0.575 and 0.825, respectively, and the IDI increased significantly by 0.280 and 0.398, respectively.

Conclusions: Radiomics of preoperative multi-sequence MRI can improve the predictive performance of MVI in HCC.

Keywords: Radiomics; Magnetic resonance imaging; Microvascular invasion; Hepatocellular carcinoma; Predictive performance

Introduction

Hepatocellular carcinoma (HCC) is the sixth most common cancer worldwide and the third leading cause of cancer-related death [1, 2]. In 2020, there were 905,677 new cases and 830,180 new deaths in the world [2]. New HCC cases and deaths in China account for about 50% of the world [3]. The etiology of liver disease is crucial, as recent studies have revealed how it impacts the development and prognosis of HCC [4]. For HCC patients with well-preserved liver function and solitary neoplasm, surgical resection is the optimal treatment [5]. However, tumor recurrence within 5 years after hepatectomy is as high as 70%, and even liver transplantation is as high as 20% [6-9]. Studies have shown that microvascular invasion (MVI) is an independent risk factor for recurrence and poor prognosis of HCC after surgical resection or transplantation [10, 11].

MVI has a reported incidence of 15-57% according to

different diagnostic criteria and study population [12, 13]. Accurate preoperative prediction of MVI is of great significance to the individualized treatment decision of HCC. For HCC patients with MVI, liver transplantation is not recommended according to the new Milan criteria [14], and surgical resection is recommended anatomical hepatectomy or partial hepatectomy with wide resection margin [15]. In addition, for small HCC with MVI, the early recurrence rate of surgical resection group was significantly lower than that of radiofrequency ablation group [16]. However, the gold standard for MVI is pathological biopsy, it is invasive and lags behind. Therefore, a new method for preoperative evaluation of MVI status is needed [17].

Enhanced magnetic resonance imaging (MRI) demonstrates strong predictive capabilities for MVI. The heightened sensitivity of hepatobiliary contrast agent-based MRI in diagnosing small HCC cases lacking arterial enhancement is of utmost importance for early HCC detection, ultimately reducing the incidence of HCC with MVI [18]. Many studies have reported multiple MRI features to predict MVI of HCC, including large tumor diameter [19], non-smooth margin [20, 21], non-radiological capsule enhancement [22], arterial peritumoral enhancement [16, 21], rim arterial phase hyperenhancement [23], and non-peripheral "washout" [22, 24]. But these imaging features are subjective and different between observers. Radiomics is an emerging field. It performs high-throughput data mining and quantification from radiological images, which provides important explanations for cancer phenotypes and tumor microenvironment [25, 26]. This is a noninvasive and objective method that can predict MVI of HCC preoperatively (before surgery).

In recent years, there have been many studies on the prediction of MVI by radiomics, and many radiomics models have been established. However, compared with the traditional model, there is no report on the improvement of the prediction accuracy of the radiomics model. The purpose of this study was to demonstrate the value of radiomics in predicting MVI of HCC.

Materials and Methods

Study participants

This retrospective study was approved by the Ethics Committee of Eastern Hepatobiliary Surgery Hospital, the Third Affiliated Hospital of Shanghai Naval Military Medical University, China, and the requirement of obtaining written informed consent was waived. The study was conducted in compliance with the ethical standards of the responsible institution on human subjects as well as with the Helsinki Declaration.

A total of 559 patients who underwent preoperative enhanced magnetic resonance (MR) for liver examination from January 2016 to January 2019 were searched in the hospital workstation. Totally, 206 primary HCC patients were finally recruited into this research (mean age: 55.19 ± 10.69 years, 34 women and 172 men). The inclusion criteria were as follows: 1) The pathological diagnosis was HCC, and the treatment option was surgical resection; 2) Enhanced MR within 1 month before hepatectomy and with suitable image quality; 3) MVI status is

reported in pathological report; 4) The preoperative imaging examination and postoperative pathological results showed that there was no macrovascular invasion, no bile duct tumor thrombosis or extrahepatic metastasis; 5) Without previous treatment history, such as local ablation, partial hepatectomy, radiotherapy, chemotherapy or transarterial chemoembolization. The inclusion flow chart of the study patient is shown in Figure 1.

MRI image acquisition

All MR scans were performed at a 1.5T MR (optima MR360, GE Healthcare) with eight-channel abdominal coil. After fasting for 4 h, the patient was injected with gadopentetate dimeglumine (Gd-DTPA) into the median cubitus vein, with a total dose of 0.1 mmol/kg, using a high-pressure syringe at the rate of 2.0 mL/s, and then rinsed with 20 mL physiological saline. At 35 - 45 s, 55 - 70 s and 100 - 180 s after injection of contrast agent, arterial phase (AP), portal phase (PP) and delayed phase (DP) scans were performed respectively. T1-weighted imaging (T1WI), Fat-suppressed T2-weighted imaging (T2WI) and diffusion-weighted imaging (DWI) were collected. The MRI settings used in the present study are detailed here (Supplementary Material 1, www.wjon.org).

MR imaging analysis

Two radiologists with more than 5 years' experience in abdominal MRI performed blind review of MR images of all patients. In case of disagreement, the third radiologist with more than 10 years' experience in liver MRI will be invited to join the discussion and make a decision.

A total of 12 imaging features were evaluated: 1) Tumor diameter; 2) Radiological capsule enhancement; 3) Restricted diffusion; 4) Nonrim arterial phase hyperenhancement (APHE); 5) Rim APHE; 6) Non-peripheral "washout"; 7) tumor number; 8) Shape; 9) Margin [21, 27]; 10) Enhancement pattern; 11) Arterial peritumoral enhancement [21, 28, 29]; 12) MRI liver cirrhosis. Criteria 1) to 6) were defined in LI-RADS v2018 [30], and the whole definition could be found here (Supplementary Material 2, www.wjon.org).

Clinical variables, pathologic factors, and MVI

Laboratory indexes, demographic information, and pathological results of patients were retrieved through the hospital case system.

Pathologist of the patient's Hospital evaluated the MVI of HCC by referring to the latest practice guideline for pathological diagnosis formulated in China. It was recommended that the risk be stratified according to the following quantities and distributions, as follows: M0: no MVI; M1 (low-risk): MVI of < 5 and at ≤ 1 cm away from the adjacent liver tissues; and M2 (high-risk): MVI of > 5 or at > 1 cm away from the adjacent liver tissues [31]. In our study, M0 was MVI absent, M1 and M2 were MVI present.
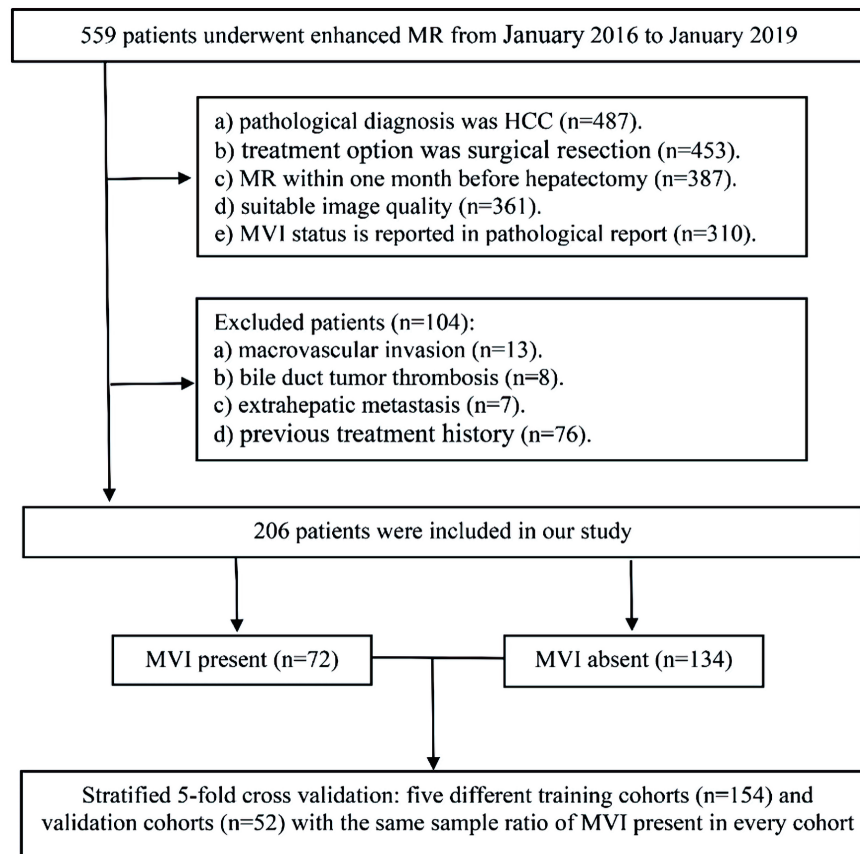
Figure 1. The workflow of patient selection for this study. MR: magnetic resonance; MVI: microvascular invasion; HCC: hepatocellular carcinoma.

Radiomics analysis of MR images

The workflow of the radiomics analysis is shown in Figure 2.

Segmentation

Three-dimensional segmentation of HCC was manually delineated by two radiologists (S.K.R and L.W.M, 5 years of experience in liver MRI), on the T1WI, T2WI, DWI with b values of 600 s/mm^2, AP, PP and DP, covering the whole tumor, by using ITK-SNAP software. Radiologist 3 (J.N.Y, 20 years of experience in liver MRI) independently validated the segmentation. We also conducted test-retest procedures on 30 randomly selected tumors. While testing the reproducibility of features extracted from repeated segmentation, features with intraclass correlation coefficients (ICCs) lower than 0.80 were also excluded [32].

Feature extraction

Before extracting features, images were resampled into a voxel size of 3 × 3 × 3 mm^3 to standardize the voxel spacing, and voxel intensity values were discretized by using a fixed bin width of 5 HU to normalize intensities and reduce image noise, enabling the normalization of image intensity values and allow acquisition of isotropic voxels [33-35]. The radiomic features were extracted using the open-source package PyRadiomics. These include shape-based features, first order statistics, and textural features including gray level co-occurrence matrix (GLCM), gray level run length matrix (GLRLM), gray level size zone matrix (GLSZM) and gray level dependence matrix (GLDM). A total of 1,046 radiomic features are extracted from each three-dimensional segmentation, resulting in 6,276 features for each lesion in total.

Radiomics feature selection

Features with ICC less than 0.8 were removed, and the remaining features were standardized by using z-scores. Recursive feature elimination (RFE) was applied to select the radiomics features of single sequence and multi-sequence fusion.

Radiomics model construction

The models of single sequence and fusion sequence were constructed by logistic regression. The optimal radiomics model
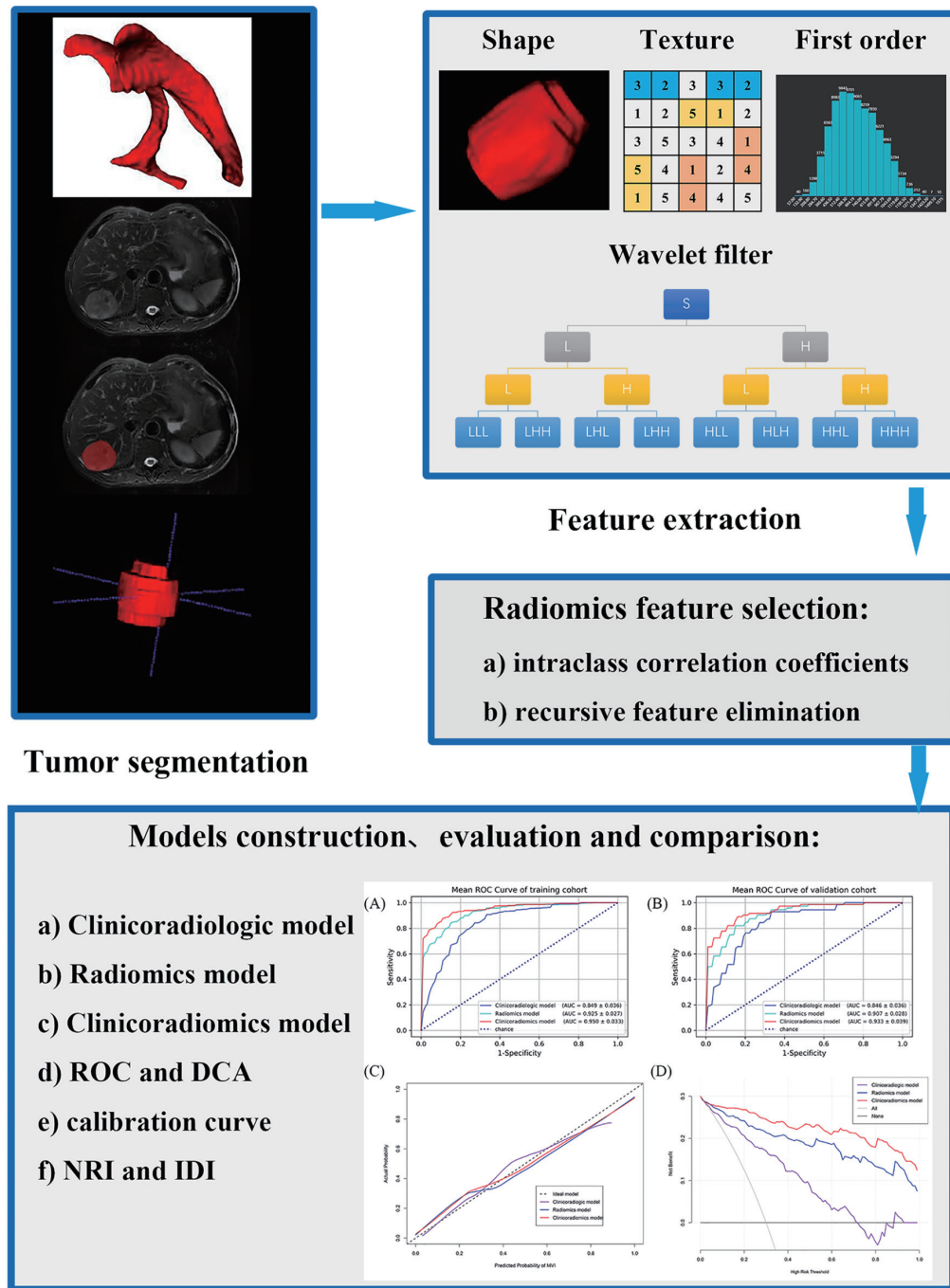
Figure 2. The workflow of the radiomics analysis. ROC: receiver operating characteristic; DCA: decision curve analysis; NRI: net reclassification improvement; IDI: integrated discrimination improvement.

was selected according to the prediction accuracy and the area under the receiver operating curve (AUC).

Clinicoradiologic model construction

The clinical and MRI features with P value less than 0.05 in the univariate logistic regression analysis were included in

the multivariate logistic regression analysis (forward logistic regression), and the selected variables were used to build the clinicoradiologic model according to expert opinions.

Models' evaluation and comparison

Three models were established to predict MVI of HCC. The

previous section introduced the clinicoradiologic model and the radiomics model. As the third model, the clinicoradiomics model was a combination of the features in the two models.

Evaluation

The discrimination was evaluated by the AUC of receiver operating characteristic (ROC). The predictive accuracy was quantified with accuracy and validated by calibration curves. The clinical utility was visualized through decision curve analysis (DCA) by quantifying the net benefits at different threshold probabilities.

Comparison

The Delong test was used to compare the statistical significance of AUC between models. The predictive accuracy improvement level and overall improvement level between the models were compared with net reclassification improvement (NRI) and integrated discrimination improvement (IDI) [36].

Statistical analysis

SPSS software (version 25.0, IBM), R software (version 3.6.0) and Python (version 3.5.6) were used for statistical analysis. In order to make the distribution of AFP (alpha-fetoprotein) and PIVKA-II (protein induced by vitamin K absence or antagonist-II) tend to be normal, lg10 transformation was performed on these two variables. ICC was used to determine the consistency of differences between observers, with ICC > 0.8 indicating good agreement.

Results

Clinicoradiological model

Clinicoradiological characteristics

It includes clinical features and MRI features of the ICC > 0.8 (Table 1). All baseline data can be found here (Supplementary Material 3, www.wjon.org). There were 206 patients in this study, including 172 males (83.5%) and 34 females (16.5%), with an average age of 55.19 ± 10.69 years. Totally, 134 patients were MVI negative, and 72 patients were MVI positive. Among the 206 patients, 181 had a history of hepatitis B (87.86%), five had hepatitis C (2.43%), one had schistosomal cirrhosis (0.49%), three had alcoholic cirrhosis (1.46%), and the remaining 16 had no history of liver disease (7.77%). Among the 78 patients with postoperative pathological confirmation of liver cirrhosis, one had schistosomal cirrhosis (1.28%), three had alcoholic cirrhosis (3.85%), and the remaining 74 had hepatitis B cirrhosis (94.87%).

Univariable logistic regression

According to the test level of P < 0.05, AFP_lg10, PIVKA-II_lg10, shape, margin, nonrim APHE, radiological capsule enhancement, rim APHE, non-peripheral "washout", enhancement pattern, arterial peritumoral enhancement and MRI liver cirrhosis were significantly related to MVI in univariate analysis (Tables 1, 2).

Multivariable logistic regression

The 11 variables selected by univariate analysis were included in multivariate logistic regression analysis (forward logistic regression), and four independent factors of MVI were screened (Table 2): AFP_lg10 (odds ratio (OR): 1.469; 95% confidence interval (CI): 1.002 - 2.154; P = 0.049), radiological capsule enhancement (incomplete/complete: OR: 4.101, 95% CI: 1.721 - 9.770, P = 0.001; absent/complete OR: 5.193, 95% CI: 1.797 - 15.009, P = 0.002), enhancement pattern (OR: 2.793; 95% CI: 1.358 - 5.742; P = 0.005), and arterial peritumoral enhancement (OR: 8.222; 95% CI: 3.917 - 17.259; P < 0.001).

Clinicoradiological model

The above four variables form the clinicoradiological model, with the mean AUC was 0.849 in the training cohort, and 0.846 in the validation cohort after stratified five-fold cross-validation for improving prediction (Fig. 3a, b). The accuracy, sensitivity and specificity were 0.779, 0.843, 0.727 in the training cohort and 0.743, 0.930, 0.667 in the validation cohort, respectively (Table 3).

Radiomics model and clinicoradiomics model

The number of radiomics features with the best model performance of each sequence and fusion sequence was selected between 10 and 20. The radiomics model performance of single sequence and fusion sequence after stratified five-fold cross-validation is shown in Table 3. Each fold cross-validation's AUC (Supplementary Material 4, www.wjon.org) and feature names in every radiomics model could be seen here (Supplementary Material 5, 6, www.wjon.org).

Among the single sequence radiomics models, no model had better performance than the clinicoradiological model. Therefore, we combined two, three, four or all sequences to form a fusion radiomics model. After comparison, we selected all the sequence fusion model as the best radiomics model, with 18 radiomics features. The mean AUC (Fig. 3c, d), accuracy, sensitivity and specificity were 0.925, 0.883, 0.844, 0.848 in the training cohort and 0.907, 0.820, 0.820, 0.848 in the validation cohort, respectively (Table 3).

Four clinicoradiological variables and 18 radiomics features constituted clinicoradiomics model. The mean AUC (Fig. 3e, f), accuracy, sensitivity and specificity were 0.950, 0.779,

Table 1. Baseline Characteristics for Predicting MVI

Characteristic	Total (n = 206)	MVI absent (n = 134)	MVI present (n = 72)	Univariable logistic regression OR (95%CI)	P
Clinical features					
Age	55.19 ± 10.69	54.69 ± 10.85	56.13 ± 10.38	1.013 (0.986, 1.041)	0.357
Gender					
Male	172 (83.5%)	108 (52.4%)	64 (31.1%)		
Female	34 (16.5%)	26 (12.6%)	8 (3.9%)	0.519 (0.222, 1.216)	0.131
BCLC stage					0.080
0	52 (25.2%)	32 (15.5%)	20 (9.7%)		
A	139 (67.5%)	96 (46.6%)	43 (20.9%)	0.717 (0.369, 1.393)	0.326
B	15 (7.3%)	6 (2.9%)	9 (4.4%)	2.400 (0.742, 7.767)	0.144
Child-Pugh stage					
A	198 (96.1%)	127 (61.7%)	71 (34.5%)		
B	8 (3.9%)	7 (3.4%)	1 (0.5%)	0.256 (0.031, 2.119)	0.206
Liver disease					
HBV	181 (87.9%)	116 (56.3%)	65 (31.6%)		
None or other	25 (12.1%)	18 (8.7%)	7 (3.4%)	0.694 (0.275, 1.749)	0.439
AFP-L3					
Negative	131 (63.7%)	87 (42.2%)	44 (21.4%)		
Positive	75 (36.4%)	47 (22.8%)	28 (13.6%)	1.178 (0.652, 2.129)	0.588
AFP_lg10	1.47 (0.66 - 2.34)	1.18 (0.52 - 2.13)	1.8 (0.99 - 2.65)	1.607 (1.175, 2.196)	0.003*
PIVKA-II_lg10	2.05 (1.52 - 2.79)	2.03 (1.44 - 2.72)	2.17 (1.67 - 2.98)	1.412 (1.004, 1.986)	0.047*
CA199 (U/mL)	16.45 (8.5 - 28.3)	17.3 (9.05 - 28.25)	15.1 (8.05 - 28.5)	0.992 (0.976, 1.008)	0.306
HBsAg					
Negative	32 (15.5%)	22 (10.7%)	10 (4.9%)		
Positive	174 (84.5%)	112 (54.4%)	62 (30.1%)	1.218 (0.542, 2.736)	0.633
Pathologic factors					
Microscopic cirrhosis					
Absent	128 (62.1%)	83 (40.3%)	45 (21.8%)		
Present	78 (37.9%)	51 (24.8%)	27 (13.1%)	0.976 (0.541, 1.763)	0.976
Satellite nodules					
Absent	183 (88.8%)	124 (60.2%)	59 (28.6%)		
Present	23 (11.2%)	10 (4.9%)	13 (6.3%)	2.732 (1.132, 6.592)	0.025*
Edmondson-Steiner grade					
I -II	26 (12.6%)	20 (9.7%)	6 (2.9%)		
III - IV	180 (87.4%)	114 (55.3%)	66 (32%)	1.930 (0.738, 5.047)	0.180
MRI features					
Tumor diameter (cm)	3 (2.18 - 4.43)	2.9 (2.2 - 4.13)	3.45 (2.03 - 5.28)	1.105 (0.945, 1.293)	0.212
Tumor number					
Solitary	188 (91.3%)	126 (61.2%)	62 (30.1%)		
Multiple	18 (8.7%)	8 (3.9%)	10 (4.9%)	2.540 (0.955, 6.756)	0.062
Shape					
Regular	125 (60.7%)	89 (43.2%)	36 (17.5%)		
Irregular	81 (39.3%)	45 (21.8%)	36 (17.5%)	1.978 (1.102, 3.549)	0.022*

Table 1. Baseline Characteristics for Predicting MVI - *(continued)*

Characteristic	Total (n = 206)	MVI absent (n = 134)	MVI present (n = 72)	Univariable logistic regression	
				OR (95%CI)	P
Margin					
Smooth	103 (50%)	78 (37.9%)	25 (12.1%)		
Non-smooth	103 (50%)	56 (27.2%)	47 (22.8%)	2.619 (1.445, 4.744)	0.002*
Radiological capsule enhancement					< 0.001*
Complete	79 (38.3%)	68 (33%)	11 (5.3%)		
Incomplete	86 (41.7%)	44 (21.4%)	42 (20.4%)	5.901 (2.747, 12.675)	< 0.001*
Absent	41 (19.9%)	22 (10.7%)	19 (9.2%)	5.339 (2.204, 12.931)	< 0.001*
Restricted diffusion					
Present	193 (93.7%)	123 (59.7%)	70 (34%)		
Absent	13 (6.3%)	11 (5.3%)	2 (1%)	0.319 (0.069, 1.483)	0.145
Nonrim APHE					
Present	123 (59.7%)	97 (47.1%)	26 (12.6%)		
Absent	83 (40.3%)	37 (18%)	46 (22.3%)	4.638 (2.515, 8.554)	< 0.001*
Rim APHE					
Absent	136 (66%)	104 (50.5%)	32 (15.5%)		
Present	70 (34%)	30 (14.6%)	40 (19.4%)	4.333 (2.337, 8.034)	< 0.001*
Non-peripheral "washout"					
Present	123 (59.7%)	92 (44.7%)	31 (15 %)		
Absent	83 (40.3%)	42 (20.4%)	41 (19.9%)	2.897 (1.602, 5.238)	< 0.001*
Enhancement pattern					
Typical	118 (57.3%)	91 (44.2%)	27 (13.1%)		
Atypical	88 (42.7%)	43 (20.9%)	45 (21.8%)	3.527 (1.937, 6.423)	< 0.001*
Arterial peritumoral enhancement					
Absent	134 (65%)	109 (52.9%)	25 (12.1%)		
Present	72 (35%)	25 (12.1%)	47 (22.8%)	8.197 (4.273, 15.723)	< 0.001*
MRI liver cirrhosis					
Absent	57 (27.7%)	44 (21.4%)	13 (6.3%)		
Present	149 (72.3%)	90 (43.7%)	59 (28.6%)	2.219 (1.101, 4.470)	0.026*

*P < 0.05. The original units of lg10 converted variables are AFP (ng/L), PIVKA-II (mAU/mL). P is the P value of univariate logistic regression analysis. MVI: microvascular invasion; OR: odd ratio; CI: confidence interval; BCLC: Barcelona Clinic Liver Cancer; HBV: hepatitis B virus; AFP: alpha-fetoprotein; PIVKA-II: protein induced by vitamin K absence or antagonist-II; CA199: carbohydrate antigen 19-9; APHE: arterial phase hyperenhancement; MRI: magnetic resonance imaging.

0.879, 0.889 in the training cohort and 0.933, 0.869, 0.890, 0.839 in the validation cohort, respectively (Table 3).

Performance and clinical practicability of the three models

The three models have good discrimination (Fig. 4a, b) after stratified five-fold cross-validation and the calibration curves (Fig. 4c) show that the predicted MVI present probability of the three models is consistent with the estimated value of the actual MVI present probability.

The DCA curve of the three models is shown in Figure 4d, the black dotted line represents the hypothesis that all patients have MVI, and the black solid line represents the assumption that no patient has MVI; these are two extreme conditions. The purple solid line represents the clinicoradiological model, the blue solid line represents the radiomics model, and the red solid line represents the clinicoradiomics model. In the DCA, when the threshold probability is greater than 5%, the net benefit of the three models for predicting MVI of HCC is higher than the two extreme conditions, indicating that these models have potential clinical benefits. At the same time, the clinical net benefit of clinicoradiomics model is higher than radiomics model, and the radiomics model is higher than clinicoradiological model, which indicates that radiomics has a very large potential clinical benefit.

Table 2. Univariate and Multivariate Logistic Regression Analysis for Predicting MVI

Variable	Univariable logistic regression			Multivariable logistic regression		
	OR	95% CI	P	OR	95% CI	P
AFP_lg10	1.607	1.175, 2.196	0.003	1.469	1.002, 2.154	0.049
PIVKA-II_lg10	1.412	1.004, 1.986	0.047			
Shape (irregular)	1.978	1.102, 3.549	0.022			
Margin (non-smooth)	2.619	1.445, 4.744	0.002			
Radiological capsule enhancement			< 0.001			0.002
Incomplete	5.901	2.747, 12.675	< 0.001	4.101	1.721, 9.770	0.001
Absent	5.339	2.204, 12.931	< 0.001	5.193	1.797, 15.009	0.002
Nonrim APHE (absent)	4.638	2.515, 8.554	< 0.001			
Rim APHE (present)	4.333	2.337, 8.034	< 0.001			
Non-peripheral "washout" (absent)	2.897	1.602, 5.238	< 0.001			
Enhancement pattern (atypical)	3.527	1.937, 6.423	< 0.001	2.793	1.358, 5.742	0.005
Arterial peritumoral enhancement (present)	8.197	4.273, 15.723	< 0.001	8.222	3.917, 17.259	< 0.001
MRI liver cirrhosis (present)	2.219	1.101, 4.470	0.026			

P is the P value of univariate and multivariate logistic regression analysis. MVI: microvascular invasion; OR: odd ratio; CI: confidence interval; AFP: alpha-fetoprotein; PIVKA-II: protein induced by vitamin K absence or antagonist-II; APHE: arterial phase hyperenhancement; MRI: magnetic resonance imaging.

Comparison between models

It can be seen from the mean ROC curve (Fig. 4a, b) and decision curve (Fig. 4d) of the three models that the prediction performance of clinicoradiologic, radiomics and clinicoradiomics model is getting better and better, and radiomics plays an important role in improving the prediction performance of MVI. However, the predictive value of radiomics cannot be quantified and proved to be statistically significant. Therefore, we introduced NRI and IDI to demonstrate that radiomics can indeed improve the predictive performance of MVI in HCC and quantify its value.

The radiomics model outperformed the clinicoradiologic model (AUCs: 0.925 vs. 0.849, Delong test P = 0.0017). The proportion of correct reclassification of radiomics model was higher than clinicoradiologic model (NRI = 57.5%, P = 0.0014). The predictive performance of the radiomics model was 28% better than that of the clinicoradiologic model (IDI = 28%, P < 0.05).

The clinicoradiomics model was superior to the clinicoradiologic model (AUCs: 0.950 vs. 0.849, Delong test P < 0.0001), the proportion of correct reclassification was higher (NRI = 82.5%, P < 0.0001), and the predictive performance was also better (IDI = 39.8%, P < 0.05).

The discrimination of the clinicoradiomics model was better than that of the radiomics model (AUCs: 0.950 vs. 0.925, Delong test P = 0.0122). Not only the accuracy of reclassification prediction was improved by 31.3% (NRI = 31.3%, P = 0.0085), but also the accuracy of prediction was improved by 11.7% (IDI = 11.7%, P < 0.05).

The results show that both the models established by the radiomics itself and the models with the radiomics features are of great significance to improve the diagnostic efficiency. The

detailed parameters of model comparison are shown in Table 4.

Discussion

In order to explore whether radiomics of preoperative multisequence MRI can improve the predictive performance of MVI in HCC, three models were established and validated by stratified five-fold cross-validation. A traditional clinicoradiologic model with clinical and MRI features, a radiomics model with only radiomics characteristics, and a clinicoradiomics model with a combination of the first two models.

Elevated AFP_lg10 level [32, 37, 38], incomplete or absent radiological capsule enhancement [37, 39], atypical enhancement pattern and arterial peritumoral enhancement [32, 37, 39, 40] were independent risk factors for predicting MVI and composed the clinicoradiologic model. In addition to atypical enhancement patterns, other independent risk factors have been reported in previous studies. Atypical enhancement pattern refers to other enhancement patterns except "washin" in AP and "washout" in PP. It contains more imaging information than nonrim APHE and non-peripheral "washout", and it is a description of the dynamic enhancement process. In univariate logistic regression analysis, these three factors were all related to MVI, but in multivariate logistic regression analysis, only enhancement pattern was included in the final model, which was in line with our expectations. Due to the overlapping image information, only zero or one of these three variables could enter the clinicoradiologic model.

Our study established a radiomics model with 18 radiomics features screened from six MR sequences (T1WI, T2WI, DWI, AP, PP, DP), extracted from original and derived images. Eight first order statistics describe the distribution of voxel intensities
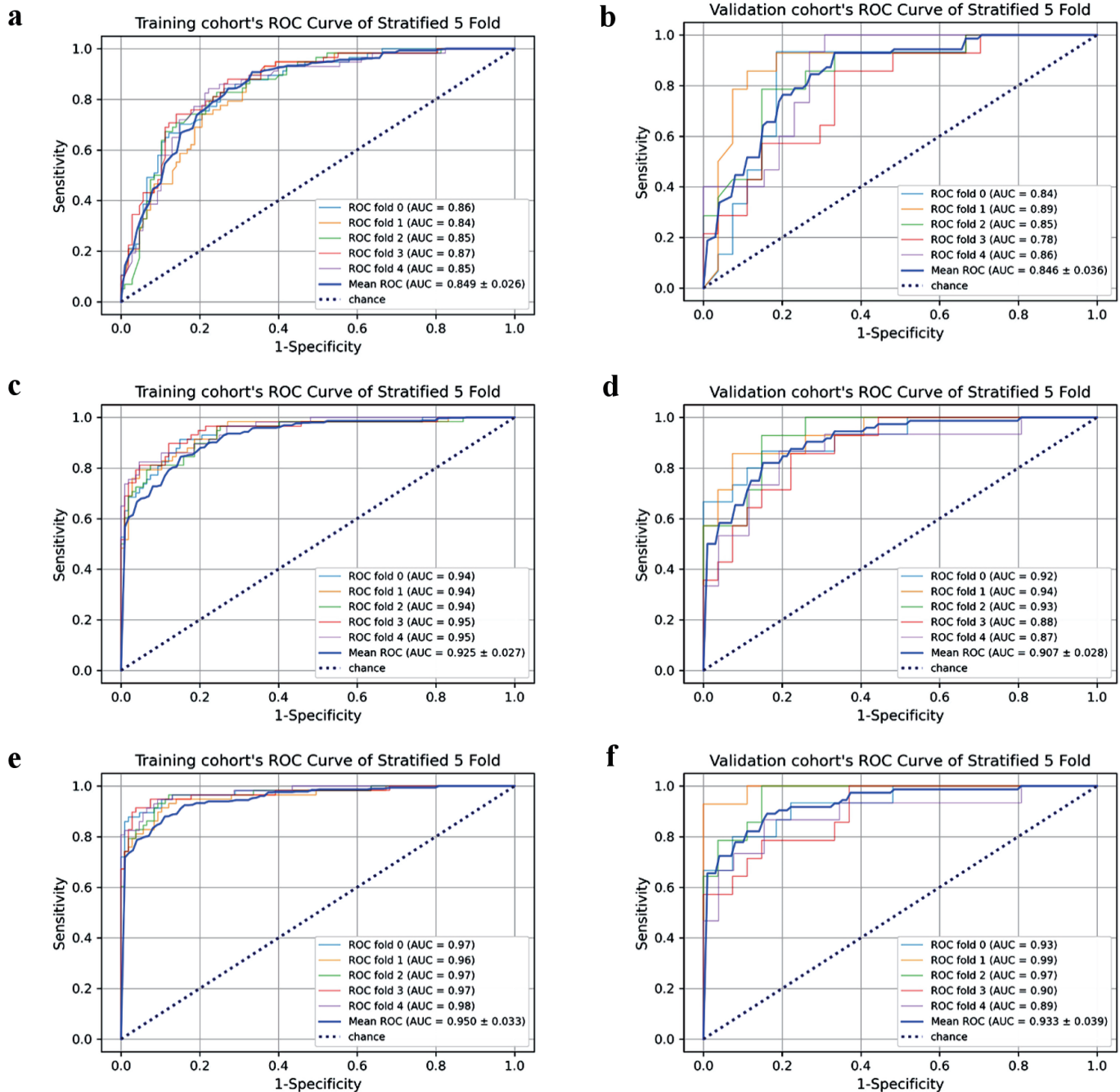
Figure 3. Each fold cross-validation's AUC and mean AUC in training/validation cohort of the three models. Clinicoradiological model's training cohort (a) and validation cohort (b). Radiomics model's training cohort (c) and validation cohort (d). Clinicoradiomics model's training cohort (e) and validation cohort (f). AUC: area under the receiver operating curve; ROC: receiver operating characteristic.

within the image region defined by the mask through commonly used and basic metrics [40]. PP_wavelet-LLH_firstorder_Maximum and PP_wavelet-HLL_firstorder_Maximum represent the maximum gray level intensity within the region of interest (ROI); AP_wavelet-LHL_firstorder_90Percentile represents the 90th percentile of all voxels in the ROI in the AP; PP_wavelet-HLH_firstorder_InterquartileRange is the 75th percentile mi-

nus the 25th percentile of the image array; T1_wavelet-LLH_firstorder_Kurtosis and T1_wavelet-HLH_firstorder_Kurtosis, represent the "peakedness" of the distribution of values in the image ROI, a higher kurtosis implies that the mass of the distribution is concentrated towards the tail(s) rather than towards the mean, a lower kurtosis implies the reverse: that the mass of the distribution is concentrated towards a spike near the mean value;

Table 3. The Mean Performances of Diverse Sequences After Stratified 5-Fold Cross-Validation for Predicting MVI

Sequences (feature number)/model	AUC		f1_score		Accuracy		Sensitivity		Specificity	
	Training	Validation	Training	Validation	Training	Validation	Training	Validation	Training	Validation
AP (20)	0.842	0.805	0.721	0.624	0.825	0.767	0.667	0.610	0.848	0.838
PP (15)	0.831	0.808	0.635	0.539	0.778	0.718	0.839	0.817	0.697	0.697
DP (13)	0.808	0.777	0.634	0.542	0.783	0.738	0.688	0.653	0.808	0.808
DWI (14)	0.827	0.802	0.634	0.526	0.609	0.743	0.827	0.750	0.697	0.778
T2 (13)	0.772	0.736	0.612	0.429	0.584	0.694	0.693	0.734	0.727	0.667
T1 (16)	0.810	0.770	0.626	0.596	0.647	0.576	0.683	0.610	0.778	0.798
AP + DWI (16)	0.870	0.855	0.711	0.671	0.818	0.786	0.708	0.634	0.848	0.919
AP + PP (17)	0.855	0.819	0.746	0.616	0.842	0.762	0.673	0.628	0.889	0.889
AP + DP (15)	0.845	0.823	0.680	0.639	0.805	0.776	0.721	0.749	0.798	0.737
PP + DP (17)	0.854	0.810	0.719	0.618	0.824	0.772	0.702	0.791	0.838	0.667
PP + DWI (18)	0.872	0.855	0.720	0.659	0.822	0.787	0.770	0.807	0.848	0.798
T1 + T2 (20)	0.857	0.824	0.726	0.626	0.830	0.762	0.813	0.903	0.737	0.667
AP + PP + DP (15)	0.859	0.835	0.718	0.669	0.822	0.791	0.727	0.791	0.838	0.737
AP + PP + DWI (19)	0.889	0.860	0.783	0.656	0.858	0.777	0.857	0.834	0.778	0.768
AP + DP + DWI (20)	0.916	0.897	0.809	0.788	0.876	0.859	0.803	0.790	0.889	0.889
PP + DP + DWI (20)	0.906	0.878	0.810	0.712	0.881	0.815	0.813	0.831	0.848	0.778
AP + PP + DP + DWI (20)	0.920	0.904	0.829	0.707	0.888	0.811	0.824	0.790	0.889	0.879
ALL/radiomics (18)	0.925	0.907	0.823	0.722	0.883	0.820	0.844	0.820	0.848	0.848
Clinicoradiologic	0.849	0.846	0.643	0.576	0.779	0.743	0.843	0.930	0.727	0.667
Clinicoradiomics	0.950	0.933	0.887	0.812	0.779	0.869	0.879	0.890	0.889	0.838

The training and validation cohort's performances of each fold for predicting MVI was shown here (Supplementary Material 5, www.wjon.org). ALL = (AP + PP + DP + DWI + T1 + T2), was also the radiomics model. MVI: microvascular invasion; AUC: area under receiver operating characteristic curve; T2: T2-weighted imaging; T1: T1-weighted imaging; DWI: diffusion-weighted imaging; AP: arterial phase; PP: portal phase; DP: delayed phase.

DP_wavelet-HHL_firstorder_Skewness and T2_log-sigma-5-0-mm-3D_firstorder_Skewness represent the asymmetry of the distribution of values about the mean value [41].

The other 10 radiomics features produced by texture analysis also contain important information, which may reflect the heterogeneity of MVI-present and MVI-absent HCCs [32, 42]. DP_wavelet-HHH_glcm_ClusterShade and DWI_wavelet-HLL_glcm_ClusterShade, are measures of the skewness and uniformity of the GLCM, the higher the cluster shadow, the greater the asymmetry of the mean value; PP_log-sigma-3-0-mm-3D_glcm_DifferenceVariance and DP_wavelet-LHL_glcm_DifferenceVariance are a measure of heterogeneity that places higher weights on differing intensity level pairs that deviate more from the mean; DP_wavelet-HLH_glcm_Autocorrelation represents the magnitude of the fineness and coarseness of texture; DWI_original_glcm_InverseVariance represents heterogeneity [41, 43]. T1_wavelet-LHL_glszm_SizeZoneNonUniformityNormalized measures the variability of size zone volumes throughout the image, with a lower value indicating more homogeneity among zone size volumes in the image; T1_log-sigma-3-0-mm-3D_glszm_LargeAreaLowGrayLevelEmphasis and T1_log-sigma-4-0-mm-3D_glszm_SmallAreaLowGray-LevelEmphasis measure the proportion in the image of the joint distribution of larger/smaller size zones with lower gray-level values; AP_wavelet-HLL_gldm_LargeDependenceHighGray-LevelEmphasis measures the joint distribution of large dependence with higher gray-level values [41, 44].

The radiomics approach possesses fundamental strengths, demonstrating the ability to predict specific factors with a high degree of accuracy and serving as a predictive biomarker, all while remaining noninvasive [45]. In contrast to numerous studies focused on biomarkers primarily prognostic in nature [46-48], informing patients about their life expectancy, radiomics, as a predictive biomarker, offers crucial insights associated with treatments, thereby directly impacting patients' well-being. Our current study illustrates the predictive potential of radiomics in forecasting MVI in HCC. This predictive capacity results in significant alterations in patient management, particularly in the choice of surgical interventions, firmly establishing it as a predictive biomarker. Furthermore, the noninvasive nature of clinicoradiomics enables longitudinal assessments, allowing for multiple evaluations over time.

In the past 2 years, more and more studies on predicting MVI by radiomics analysis of HCC have been published [13]. A meta-analysis about radiomics for the preoperative evaluation of MVI in HCC showed high pooled sensitivity (0.84;
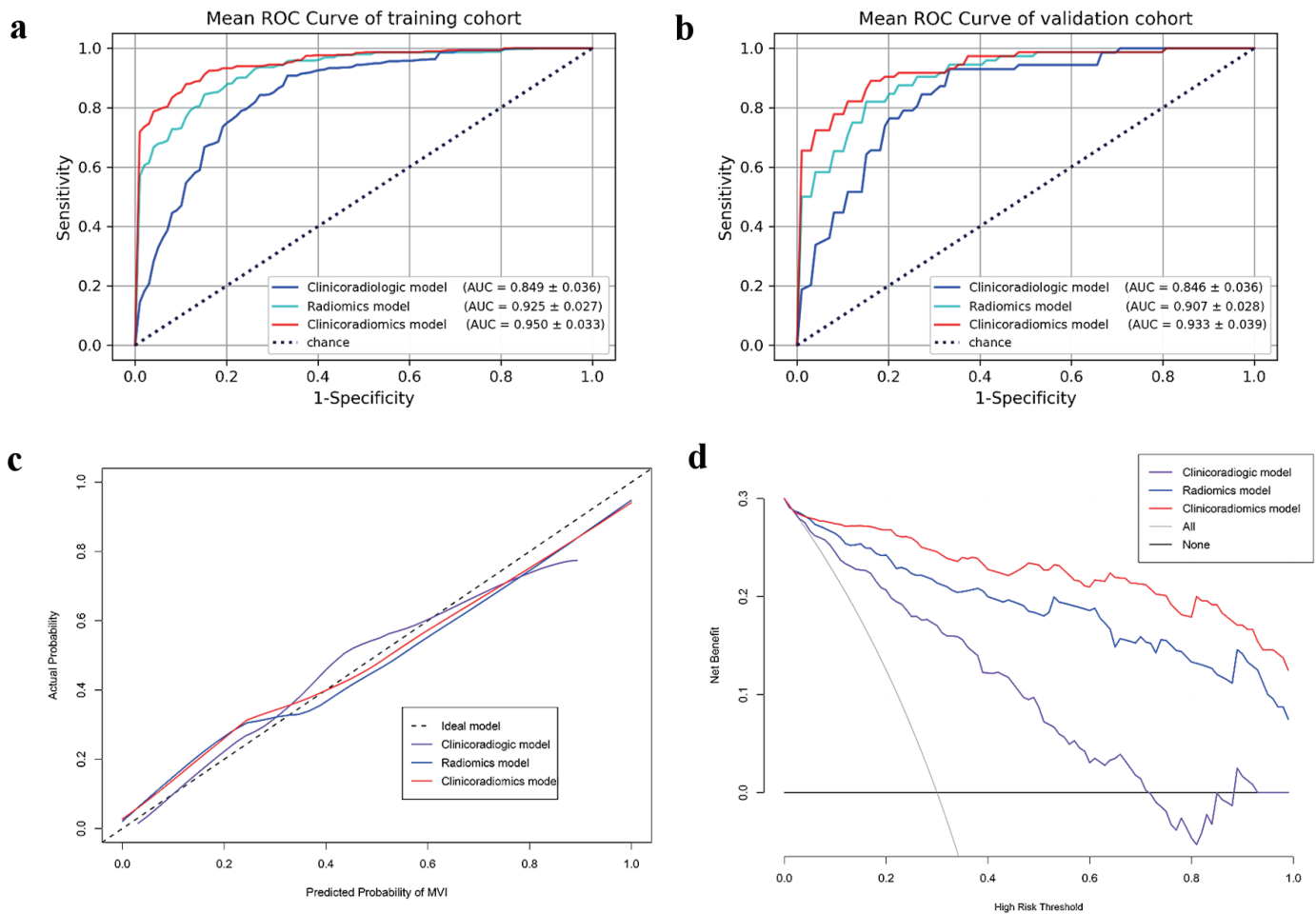
Figure 4. The three models' mean ROC curves of training cohort (a) and validation cohort (b). Calibration curves (c) and DCA curves (d) of three models for predicting MVI of HCC. AUC: area under the receiver operating curve; ROC: receiver operating characteristic; DCA: decision curve analysis; MVI: microvascular invasion; HCC: hepatocellular carcinoma.

95% CI: 0.81, 0.87), specificity (0.83; 95% CI: 0.78, 0.87), and AUC (0.90; 95% CI: 0.87, 0.92) values [17]. A systematic review of radiomics models for predicting MVI in HCC showed the added value of radiomics in imaging modalities used in clinical routines has been explored extensively, with an AUC as high as 0.80 - 0.84 in two independent validation cohorts [13]. However, in all these studies [32, 33, 37, 39, 40, 49], the radiomics scores of the corresponding subjects were obtained through the optimal radiomics model in the training cohort, combined with independent risk clinicoradiologic factors to predict MVI of HCC, and verified in the validation cohort

to prove that the model performed well. No study has shown whether the independent radiomics model can independently or even improve the predictive performance of MVI, and how much they can improve, compared with the traditional clinical or clinicoradiologic model [12, 21, 38, 50, 51]. However, our study confirmed this. Through the comparison between models, it was found that the NRI and IDI of the optimal radiomics model were 57.5% and 28.0% higher than the traditional clinicoradiologic model, respectively, with statistical significance. The NRI and IDI of the clinicoradiomics model composed of radiomics features and clinicoradiologic variables were signif-

Table 4. Comparison Between Models

	P (AUC)	NRI	P (NRI)	IDI	P (IDI)
Radiomics vs. clinicoradiologic	0.0017	0.575	0.0014	0.280	< 0.05
Clinicoradiomics vs. clinicoradiologic	< 0.0001	0.825	< 0.0001	0.398	< 0.05
Clinicoradiomics vs. radiomics	0.0122	0.313	0.0085	0.117	< 0.05

P is the probability when Delong test is used to compare the ROC curve of two models. AUC: area under receiver operating characteristic curve; NRI: net reclassification improvement; IDI: integrated discrimination improvement.

icantly higher than the clinicoradiologic model by 82.5% and 39.8%, respectively, with statistical significance. This not only shows that radiomics of preoperative multi-sequence MRI can indeed improve the predictive performance of MVI in HCC, but also provides strong data support.

This study also has limitations. First, this is a retrospective study with possible selective bias. Second, this is a single-center study, and multi-center datasets should be used in subsequent studies to verify the results. Third, instead of using internal validation that divides the data into real training and validation cohorts, we used the stratified five-fold cross-validation to take full advantage of the data and balance the interclass bias, which may have some overfitting.

In conclusion, this study demonstrates that radiomics of preoperative multi-sequence MRI can indeed improve the predictive performance of MVI in HCC. We need to pay more attention to the role of radiomics in predicting MVI.

Learning points

Clinicoradiologic model, radiomics model, and clinicoradiomics model were established respectively.

Through the comparison between models, it was found that the radiomics of preoperative multi-sequence MRI can indeed improve the predictive performance of MVI in HCC.

It is important to emphasize the significance of radiomics in predicting MVI.

Supplementary Material

Suppl 1. Sequences and parameters of MRI
Suppl 2. The definition of LI-RADS v2018 imaging features
Suppl 3. Baseline characteristics for predicting MVI.
Suppl 4. The violin plot of AUC for each fold cross-validation of single sequence and fused sequence.
Suppl 5. The performances of each fold cross-validation for predicting MVI
Suppl 6. Feature names in every radiomics model

Acknowledgments

None to declare.

Financial Disclosure

Conflict of Interest

The authors declare that the research was conducted in the ab-

sence of any commercial or financial relationships that could be construed as a potential conflict of interest.

Informed Consent

This retrospective study was approved by the Ethics Committee of Eastern Hepatobiliary Surgery Hospital, the Third Affiliated Hospital of Shanghai Naval Military Medical University, China, and the requirement of obtaining written informed consent was waived.

Author Contributions

All authors contributed to the study conception and design. Material preparation and data collection were performed by Meng Ting Gu, Hui Lin Chen, Kai Rong Song, Wei Zheng and Hui Yu. Analyses were performed by Ai E Liu and Wan Min Liu. The first draft of the manuscript was written by Wan Min Liu and Xing Yu Zhao. Xiang Zhou, Xiao Wen Xu, Ning Yang Jia and Pei Jun Wang revised and reviewed the article. All authors commented on previous versions of the manuscript. All authors read and approved the final manuscript.

Data Availability

The original contributions presented in the study are included in the article/supplementary material. Further inquiries can be directed to the corresponding authors.

Abbreviations

MVI: microvascular invasion; HCC: hepatocellular carcinoma; RFE: recursive feature elimination; NRI: net reclassification improvement; IDI: integrated discrimination improvement; AFP: alpha-fetoprotein; AUC: area under the receiver operating curve; DCA: decision curve analysis; MRI: magnetic resonance imaging; Gd-DTPA: gadopentetate dimeglumine; AP: arterial phase; PP: portal phase; DP: delayed phase T1WI, T1-weighted imaging; T2WI: T2-weighted imaging; DWI: diffusion-weighted imaging; APHE: arterial phase hyperenhancement; ICC: intraclass correlation coefficients; GLCM: gray level co-occurrence matrix; GLRLM: gray level run length matrix; GLSZM: gray level size zone matrix; GLDM: gray level dependence matrix; ROC: receiver operating characteristic; ROI: region of interest

References

1. Siegel RL, Miller KD, Fuchs HE, Jemal A. Cancer statistics, 2021. CA Cancer J Clin. 2021;71(1):7-33. doi pubmed
2. Sung H, Ferlay J, Siegel RL, Laversanne M, Soerjomataram I, Jemal A, Bray F. Global cancer statistics 2020:

GLOBOCAN estimates of incidence and mortality worldwide for 36 cancers in 185 countries. CA Cancer J Clin. 2021;71(3):209-249. doi pubmed

3. Zhou M, Wang H, Zeng X, Yin P, Zhu J, Chen W, Li X, et al. Mortality, morbidity, and risk factors in China and its provinces, 1990-2017: a systematic analysis for the Global Burden of Disease Study 2017. Lancet. 2019;394(10204):1145-1158. doi pubmed pmc

4. Garuti F, Neri A, Avanzato F, Gramenzi A, Rampoldi D, Rucci P, Farinati F, et al. The changing scenario of hepatocellular carcinoma in Italy: an update. Liver Int. 2021;41(3):585-597. doi pubmed

5. Villanueva A. Hepatocellular carcinoma. N Engl J Med. 2019;380(15):1450-1462. doi pubmed

6. Vitale A, Peck-Radosavljevic M, Giannini EG, Vibert E, Sieghart W, Van Poucke S, Pawlik TM. Personalized treatment of patients with very early hepatocellular carcinoma. J Hepatol. 2017;66(2):412-423. doi pubmed

7. Gunasekaran G, Bekki Y, Lourdusamy V, Schwartz M. Surgical treatments of hepatobiliary cancers. Hepatology. 2021;73(Suppl 1):128-136. doi pubmed

8. Fujiwara N, Friedman SL, Goossens N, Hoshida Y. Risk factors and prevention of hepatocellular carcinoma in the era of precision medicine. J Hepatol. 2018;68(3):526-549. doi pubmed pmc

9. Llovet JM, Schwartz M, Mazzaferro V. Resection and liver transplantation for hepatocellular carcinoma. Semin Liver Dis. 2005;25(2):181-200. doi pubmed

10. Sheng X, Ji Y, Ren GP, Lu CL, Yun JP, Chen LH, Meng B, et al. A standardized pathological proposal for evaluating microvascular invasion of hepatocellular carcinoma: a multicenter study by LCPGC. Hepatol Int. 2020;14(6):1034-1047. doi pubmed

11. Hong SB, Choi SH, Kim SY, Shim JH, Lee SS, Byun JH, Park SH, et al. MRI features for predicting microvascular invasion of hepatocellular carcinoma: a systematic review and meta-analysis. Liver Cancer. 2021;10(2):94-106. doi pubmed pmc

12. Lei Z, Li J, Wu D, Xia Y, Wang Q, Si A, Wang K, et al. Nomogram for preoperative estimation of microvascular invasion risk in hepatitis B virus-related hepatocellular carcinoma within the Milan criteria. JAMA Surg. 2016;151(4):356-363. doi pubmed

13. Wang Q, Li C, Zhang J, Hu X, Fan Y, Ma K, Sparrelid E, et al. Radiomics models for predicting microvascular invasion in hepatocellular carcinoma: a systematic review and radiomics quality score assessment. Cancers (Basel). 2021;13(22). doi pubmed pmc

14. Mazzaferro V, Llovet JM, Miceli R, Bhoori S, Schiavo M, Mariani L, Camerini T, et al. Predicting survival after liver transplantation in patients with hepatocellular carcinoma beyond the Milan criteria: a retrospective, exploratory analysis. Lancet Oncol. 2009;10(1):35-43. doi pubmed

15. Hwang S, Lee YJ, Kim KH, Ahn CS, Moon DB, Ha TY, Song GW, et al. The impact of tumor size on long-term survival outcomes after resection of solitary hepatocellular carcinoma: single-institution experience with 2558 patients. J Gastrointest Surg. 2015;19(7):1281-1290. doi

16. Lee S, Kang TW, Song KD, Lee MW, Rhim H, Lim HK, Kim SY, et al. Effect of microvascular invasion risk on early recurrence of hepatocellular carcinoma after surgery and radiofrequency ablation. Ann Surg. 2021;273(3):564-571. doi pubmed

17. Li L, Wu C, Huang Y, Chen J, Ye D, Su Z. Radiomics for the preoperative evaluation of microvascular invasion in hepatocellular carcinoma: a meta-analysis. Front Oncol. 2022;12:831996. doi pubmed pmc

18. Granito A, Galassi M, Piscaglia F, Romanini L, Lucidi V, Renzulli M, Borghi A, et al. Impact of gadoxetic acid (Gd-EOB-DTPA)-enhanced magnetic resonance on the non-invasive diagnosis of small hepatocellular carcinoma: a prospective study. Aliment Pharmacol Ther. 2013;37(3):355-363. doi pubmed

19. Ryu T, Takami Y, Wada Y, Tateishi M, Hara T, Yoshitomi M, Momosaki S, et al. A clinical scoring system for predicting microvascular invasion in patients with hepatocellular carcinoma within the milan criteria. J Gastrointest Surg. 2019;23(4):779-787. doi pubmed

20. Kim AY, Sinn DH, Jeong WK, Kim YK, Kang TW, Ha SY, Park CK, et al. Hepatobiliary MRI as novel selection criteria in liver transplantation for hepatocellular carcinoma. J Hepatol. 2018;68(6):1144-1152. doi pubmed

21. Lee S, Kim SH, Lee JE, Sinn DH, Park CK. Preoperative gadoxetic acid-enhanced MRI for predicting microvascular invasion in patients with single hepatocellular carcinoma. J Hepatol. 2017;67(3):526-534. doi pubmed

22. Witjes CD, Willemssen FE, Verheij J, van der Veer SJ, Hansen BE, Verhoef C, de Man RA, et al. Histological differentiation grade and microvascular invasion of hepatocellular carcinoma predicted by dynamic contrast-enhanced MRI. J Magn Reson Imaging. 2012;36(3):641-647. doi pubmed

23. Rhee H, An C, Kim HY, Yoo JE, Park YN, Kim MJ. Hepatocellular carcinoma with irregular rim-like arterial phase hyperenhancement: more aggressive pathologic features. Liver Cancer. 2019;8(1):24-40. doi pubmed pmc

24. Ahn SJ, Kim JH, Park SJ, Kim ST, Han JK. Hepatocellular carcinoma: preoperative gadoxetic acid-enhanced MR imaging can predict early recurrence after curative resection using image features and texture analysis. Abdom Radiol (NY). 2019;44(2):539-548. doi pubmed

25. Lambin P, Leijenaar RTH, Deist TM, Peerlings J, de Jong EEC, van Timmeren J, Sanduleanu S, et al. Radiomics: the bridge between medical imaging and personalized medicine. Nat Rev Clin Oncol. 2017;14(12):749-762. doi pubmed

26. Gillies RJ, Kinahan PE, Hricak H. Radiomics: images are more than pictures, they are data. Radiology. 2016;278(2):563-577. doi pubmed pmc

27. Ariizumi S, Kitagawa K, Kotera Y, Takahashi Y, Katagiri S, Kuwatsuru R, Yamamoto M. A non-smooth tumor margin in the hepatobiliary phase of gadoxetic acid disodium (Gd-EOB-DTPA)-enhanced magnetic resonance imaging predicts microscopic portal vein invasion, intrahepatic metastasis, and early recurrence after hepatectomy in patients with hepatocellular carcinoma. J Hepatobiliary

Pancreat Sci. 2011;18(4):575-585. doi pubmed

28. Renzulli M, Brocchi S, Cucchetti A, Mazzotti F, Mosconi C, Sportoletti C, Brandi G, et al. Can current preoperative imaging be used to detect microvascular invasion of hepatocellular carcinoma? Radiology. 2016;279(2):432-442. doi pubmed

29. Chernyak V, Fowler KJ, Kamaya A, Kielar AZ, Elsayes KM, Bashir MR, Kono Y, et al. Liver imaging reporting and data system (LI-RADS) Version 2018: imaging of hepatocellular carcinoma in at-risk patients. Radiology. 2018;289(3):816-830. doi pubmed pmc

30. American College of Radiology. CT/MRI liver imaging reporting and data system v2018 core. https://www.acr.org/Clinical-Resources/Reporting-and-Data-Systems/LI-RADS/CT-MRI-LI-RADS-v2018. [Accessed Dec 28, 2021].

31. Cong WM, Bu H, Chen J, Dong H, Zhu YY, Feng LH, Chen J, et al. Practice guidelines for the pathological diagnosis of primary liver cancer: 2015 update. World J Gastroenterol. 2016;22(42):9279-9287. doi pubmed pmc

32. Yang L, Gu D, Wei J, Yang C, Rao S, Wang W, Chen C, et al. A radiomics nomogram for preoperative prediction of microvascular invasion in hepatocellular carcinoma. Liver Cancer. 2019;8(5):373-386. doi pubmed pmc

33. Gao L, Xiong M, Chen X, Han Z, Yan C, Ye R, Zhou L, et al. Multi-region radiomic analysis based on multi-sequence MRI can preoperatively predict microvascular invasion in hepatocellular carcinoma. Front Oncol. 2022;12:818681. doi pubmed pmc

34. van Griethuysen JJM, Fedorov A, Parmar C, Hosny A, Aucoin N, Narayan V, Beets-Tan RGH, et al. Computational radiomics system to decode the radiographic phenotype. Cancer Res. 2017;77(21):e104-e107. doi pubmed pmc

35. Zwanenburg A, Vallieres M, Abdalah MA, Aerts H, Andrearczyk V, Apte A, Ashrafinia S, et al. The image biomarker standardization initiative: standardized quantitative radiomics for high-throughput image-based phenotyping. Radiology. 2020;295(2):328-338. doi pubmed pmc

36. Vickers AJ, Elkin EB. Decision curve analysis: a novel method for evaluating prediction models. Med Decis Making. 2006;26(6):565-574. doi pubmed pmc

37. Chong HH, Yang L, Sheng RF, Yu YL, Wu DJ, Rao SX, Yang C, et al. Multi-scale and multi-parametric radiomics of gadoxetate disodium-enhanced MRI predicts microvascular invasion and outcome in patients with solitary hepatocellular carcinoma </= 5 cm. Eur Radiol. 2021;31(7):4824-4838. doi pubmed pmc

38. Jiang H, Wei J, Fu F, Wei H, Qin Y, Duan T, Chen W, et al. Predicting microvascular invasion in hepatocellular carcinoma: A dual-institution study on gadoxetate disodium-enhanced MRI. Liver Int. 2022;42(5):1158-1172. doi pubmed pmc

39. Xu X, Zhang HL, Liu QP, Sun SW, Zhang J, Zhu FP, Yang G, et al. Radiomic analysis of contrast-enhanced CT predicts microvascular invasion and outcome in hepatocel-

lular carcinoma. J Hepatol. 2019;70(6):1133-1144. doi pubmed

40. Yang Y, Fan W, Gu T, Yu L, Chen H, Lv Y, Liu H, et al. Radiomic features of multi-ROI and multi-phase MRI for the prediction of microvascular invasion in solitary hepatocellular carcinoma. Front Oncol. 2021;11:756216. doi pubmed pmc

41. Zwanenburg A, Leger S, Vallieres M, Lock S, Initiative F. Image biomarker standardisation initiative. 2016.

42. Chong H, Gong Y, Pan X, Liu A, Chen L, Yang C, Zeng M. Peritumoral dilation radiomics of gadoxetate disodium-enhanced MRI excellently predicts early recurrence of hepatocellular carcinoma without macrovascular invasion after hepatectomy. J Hepatocell Carcinoma. 2021;8:545-563. doi pubmed pmc

43. Haralick RM, Shanmugam K, Dinstein I. Textural features for image classification. Studies in media and communication. 1973;SMC-3(6):610-621.

44. Thibault G, Fertil B, Navarro C, et al. Texture indexes and gray level size zone matrix. Application to cell nuclei classification. Paper presented at: International Conference on Pattern Recognition 2009.

45. Taha NA, Shafiq AM, Mohammed AH, Zaky AH, Omran OM, Ameen MG. FOS-like antigen 1 expression was associated with survival of hepatocellular carcinoma patients. World J Oncol. 2023;14(4):285-299. doi pubmed pmc

46. Warli SM, Putrantyo, II, Laksmi LI. Correlation between tumor-associated collagen signature and fibroblast activation protein expression with prognosis of clear cell renal cell carcinoma patient. World J Oncol. 2023;14(2):145-149. doi pubmed pmc

47. Chen S, Pan TY, Wu X, Li T, Wei Y, He HL, Zhou XM, et al. Uses of vascular endothelial growth factor C as a lung adenocarcinoma prognostic biomarker. World J Oncol. 2023;14(1):51-59. doi pubmed pmc

48. Desai S, Guddati AK. Carcinoembryonic antigen, carbohydrate antigen 19-9, cancer antigen 125, prostate-specific antigen and other cancer markers: a primer on commonly used cancer markers. World J Oncol. 2023;14(1):4-14. doi pubmed pmc

49. Renzulli M, Mottola M, Coppola F, Cocozza MA, Malavasi S, Cattabriga A, Vara G, et al. Automatically extracted machine learning features from preoperative CT to early predict microvascular invasion in HCC: The role of the zone of transition (ZOT). Cancers (Basel). 2022;14(7). doi pubmed pmc

50. Tang M, Zhou Q, Huang M, Sun K, Wu T, Li X, Liao B, et al. Nomogram development and validation to predict hepatocellular carcinoma tumor behavior by preoperative gadoxetic acid-enhanced MRI. Eur Radiol. 2021;31(11):8615-8627. doi pubmed

51. Zhang K, Xie SS, Li WC, Ye ZX, Shen ZW, Shen W. Prediction of microvascular invasion in HCC by a scoring model combining Gd-EOB-DTPA MRI and biochemical indicators. Eur Radiol. 2022;32(6):4186-4197. doi pubmed